scientific reports

Check for updates

OPEN

Investigation on the formation of two dimensional perovskite nanostructures at the water surface through self initiated reaction

Subhadip Chowdhury[1,2], Mrinmay K Mukhopadhyay[1,2]✉, Milan K Sanyal[1]✉, Satyaban Bhunia[1,2], Biswarup Satpati[1,2], Rajendra P Giri[3,4], B. Bharatiya[5], Chen Shen[5] & Bridget M. Murphy[3,6]

The emerging class of hybrid organic-inorganic perovskites (HOIPs) has exhibited fascinating properties for a wide range of technological applications. With halide ions, HOIPs have provided novel optoelectronic devices including efficient solar cells and with pseudohalide anions-like formate ($HCOO^-$), enigmatic electromagnetic properties have been obtained in HOIPs. Large-scale synthesis of such 2D HOIP films is of immense importance for the advancement of its application as solar materials. We have shown using in-situ X-ray measurements that the Langmuir monolayer of perovskite can be formed at the air-water interface by spreading stearic acid molecules on the water subphase having $(C_4H_9NH_3)_2PbBr_4$ molecules. The 2D lead formate perovskite films are formed at the air-water interface through a self-initiated reaction and the in-situ X-ray scattering and ex-situ Raman spectroscopy measurements revealed this reaction process. The spreading of lipid molecules having positive and negative head-group charges as surfactants over the water surface shows that the formation of perovskite nanofilms at the air-water interface specifically requires the presence of $HCOO^-$ head-group of stearic acid. In this room temperature interfacial reaction, formate anions come from the stearic acid monolayer present on the water surface and completely replace bromines in the perovskite present in water subphase to form $(BA)_2Pb(HCOO)_4$ at the air-water interface. Our results show an easy route for large-scale synthesis of 2D pseudohalide perovskites.

Keywords Surface-initiated reaction, Langmuir monolayer, Liquid surface x-ray scattering, 2D hybrid organic-inorganic perovskite, White light photoluminescence

Understanding chemical reactivity at the water surface is of fundamental importance in several research areas including biology because the effect of the inhomogeneous environment can alter the behavior of the reacting molecules[1]. The hydrogen bonds in the aqueous surface and the transfer of ions/charge across liquid interfaces can be altered due to the presence of roughness, which is related to interfacial tension through capillary wave theory[2–4]. Chemical reactions at an air-liquid and a liquid-liquid interface are also a natural choice to grow free-standing anisotropic 2D structures over a large area, as this process does not require the presence of a solid substrate[5–8]. X-ray scattering techniques can probe the formation process of two-dimensional (2D) aggregates of nanoparticles of metals and compounds at the toluene-water interface[9,10]. Langmuir monolayers of a fatty acid spread on the surface of water containing metal ions and transfer of the formed monolayer to a solid substrate have been studied extensively using X-ray techniques[11,12]. Langmuir-Blodgett (LB) film growth techniques can then be used to deposit multilayer films on a solid substrate by transferring these 2D structures formed in the air-water interface through repeated dipping. Here we shall show that instead of forming simple metal salts of a fatty acid, one can form a Langmuir monolayer of a hybrid organic-inorganic perovskites (HOIP) at the air-water interface using 2D perovskite flakes[13] in the water subphase.

[1]SPMS Division, Saha Institute of Nuclear Physics, 1/AF Bidhannagar, Kolkata 700064, India. [2]Homi Bhabha National Institute, BARC Training School Complex, Anushaktinagar, Mumbai 400094, India. [3]Institut für Experimentelle und Angewandte Physik, Christian-Albrechts-Universität zu Kiel, 24098 Kiel, Germany. [4]Department of Physics, Indian Institute of Technology (ISM) Dhanbad, Jharkhand 826004, India. [5]Deutsches Elektronen-Synchrotron DESY, Notkestrasse 85, 22607 Hamburg, Germany. [6]Ruprecht-Haensel Laboratory, Kiel University, 24118 Kiel, Germany. ✉email: mrinmay.mukhopadhyay@saha.ac.in; milank.sanyal@saha.ac.in

HOIP[14–19] with the well-known ABX_3 structure, exhibited a wide range of interesting tunable properties that can be used in several technological applications. The tunability of the metal-organic framework (MOF) in ABX_3 structures arises from the fact that all three sites can be varied by keeping the B-site a metallic cation, the A-site an organic molecule, and the X-site a halogen or a polyatomic pseudohalide anion[14]. The ionic sizes of A, B, and X and the tilt of the corner-sharing BX_6 octahedra are crucial parameters to decide whether a desired perovskite can be formed[20–27] to achieve the required optical properties. The assignment of ionic radii can be straightforward for elemental inorganic ions like bromine but for non-spherical polyatomic pseudohalide anions like formate, ionic radii are calculated assuming free rotation about its center of mass using density functional theory (DFT)[14,20,28]. Among chemically diverse HOIPs, formate $AB(HCOO)_3$ exhibits a rich range of properties, such as ferromagnetism, ferro-electricity, ferro-elasticity, and non-linear optical properties[28–32]. The concept of tolerance factor becomes much more relaxed for 2D perovskites with A_2BX_4 structure—for example, there will be no restriction on the length of the A molecules[13,20,28,33].

The growth of excellent square-shaped 2D perovskite crystals has been demonstrated[13,19] from a dimethylformamide (DMF) solution of $(BA)_2PbBr_4$ where BA is butylammonium. We used the same solution in the present work to form a Langmuir monolayer of $(BA)_2Pb(HCOO)_4$ at the air-water interface by replacing bromines ($X = Br^-$) completely by the formates ($X = HCOO^-$). Though a few reports on the formation of perovskite layers through the Langmuir monolayer deposition process have been shown early[8,34], the formation of lead formate perovskites has not been observed to the best of our knowledge. The formation of such lead-formate perovskites and the effect of the headgroups in the formation of such layers through self-initiated reaction mechanisms at the air-water interface have been studied in this work. We have used three surfactants, one negatively charged small headgroup surfactant stearic acid (SA), one negatively charged headgroup lipid 1,2-dipalmitoyl-sn-glycero-3-phosphoglycerol (DPPG), and one positively charged headgroup 1,2-dipalmitoyl-sn-glycero-3-ethylphosphocholine (DPePC). Our study shows that the COOH headgroup of the SA molecule is particularly important in forming lead formate perovskite layers exhibiting well-ordered crystal structure at the air-water interface. However, the lipid headgroups do not show such perovskite layer formation even though both SA and DPPG have the same negatively charged headgroups. The positively charged head group in the DPePC lipids also do not show such perovskite layer formation. So, the specificity of the headgroups and the charge of the headgroups plays an important role in the formation of perovskites at the air-water interface. The air-water interface was monitored by in-situ X-ray reflectivity (XRR), grazing incidence X-ray diffraction (GID), and X-ray fluorescence (XRF) measurements during this interfacial reaction. The structure and optical properties of the transferred films on a Si (100) substrate and on the copper grid using the Langmuir-Schaefer (LS) deposition technique, were investigated using XRR, atomic force microscopy (AFM), transmission electron microscopy (TEM), Raman spectroscopy, and photoluminescence (PL) measurements (refer to Supporting Information (SI) for details).

Methods

Materials

Perovskite crystals $(C_4H_9NH_3)_2PbBr_4$ have been synthesized using a solution-processed method and subsequently cooling of the solution slowly (approximately 0.5 °C per minute) as described earlier[19,35,36]. A single perovskite flake consisting of multiple grains of small crystallites can be synthesized in this process with a lateral size of several tens of millimeters and a thickness of a few tens of micrometers. The solvent Dimethylformamide (DMF) was used to make a solution of these perovskite flakes.

Langmuir monolayer and x-ray scattering experiments

DMF solution of the perovskite flakes was first mixed thoroughly with water and then it was used as the water subphase for the Langmuir trough. Milli-Q water (18MΩ and pH was 7.0) was used for this purpose. Langmuir monolayer of stearic acid molecules was prepared by spreading chloroform solution of stearic acid of concentration 0.5 mg/ml on the water subphase. The Langmuir monolayer of DPPG and DPePC was prepared by spreading chloroform solution of respective lipids of concentration 0.6 mg/ml on the water subphase. The whole trough was kept in a closed enclosure to reduce water evaporation from the LB trough. A small flow of water-saturated helium gas was maintained in the trough enclosure during X-ray scattering experiments to suppress air scattering. The XRR measurements from the monolayer were performed using a monochromatic X-ray of wavelength 0.69 Å in LISA setup at the P08 beamline, PETRA-III, DESY[37,38], and the XRF, GID measurements were done using the Langmuir Trough GID setup with monochromatic x-rays of 0.83 Å in the same beamline[39].

Thin film deposition

The horizontal deposition method, the Langmuir–Schaefer (LS) method was used to prepare the perovskite thin films from the monolayer. The Si substrates were cleaned using RCA-1 and RCA-2 cleaning procedures and then hydrophobized using the HF solution etching method before deposition of the monolayer to the substrate.

Raman spectroscopy studies

Raman spectroscopy measurements from the thin films and flakes of perovskite materials were carried out using Horiba Jobin-Yvon LabRAM HR-800 spectrometer in backscattering geometry. A laser of wavelength 633 nm was used to excite the sample and the scattered light was collected by a CCD. We have performed room-temperature Raman spectroscopy for all the samples prepared.

Photoluminescence measurements

PL measurements from the LS thin films prepared from the water surface and the powder form of the crystalline flakes have been performed at 325 nm He-Cd laser from 280 K to 4 K. Horiba Jobin-Yvon iHR550 monochromator

was used and then the luminescence was collected by a photomultiplier tube for this experiment. A closed-cycle Helium cryo-cooler has been used to lower the temperature to 4 K.

AFM and TEM microscopic measurements

The AFM measurements were carried out in tapping mode using a CSI nano-observer instrument. WSXM software was used to process and analyze the AFM pictures. The TEM measurements were done using an FEI Tecnai G2F30-ST instrument operating at 300 kV. It was outfitted with a Fischione high-angle annular dark-field (HAADF) detector (model 3000) for Bragg scattering-free imaging, and an energy-dispersive X-ray (EDX) spectroscopy attachment for compositional analysis. Software called Gatan Microscopy Suite was used to examine TEM pictures.

Results and discussion

Formation of perovskite monolayer

The experimental arrangement schematically shown in Fig. 1a allowed us to monitor the changes in the air-water interface through in-situ measurements of the pressure-area (Π-A) isotherm, XRF, XRR and GID. The isotherm measurement indicates a rise in surface pressure (Π) as the area (A) available to the 2D molecular assembly forming the Langmuir monolayer reduces[8,40,41]. No change in the Π-A isotherm was observed when just the

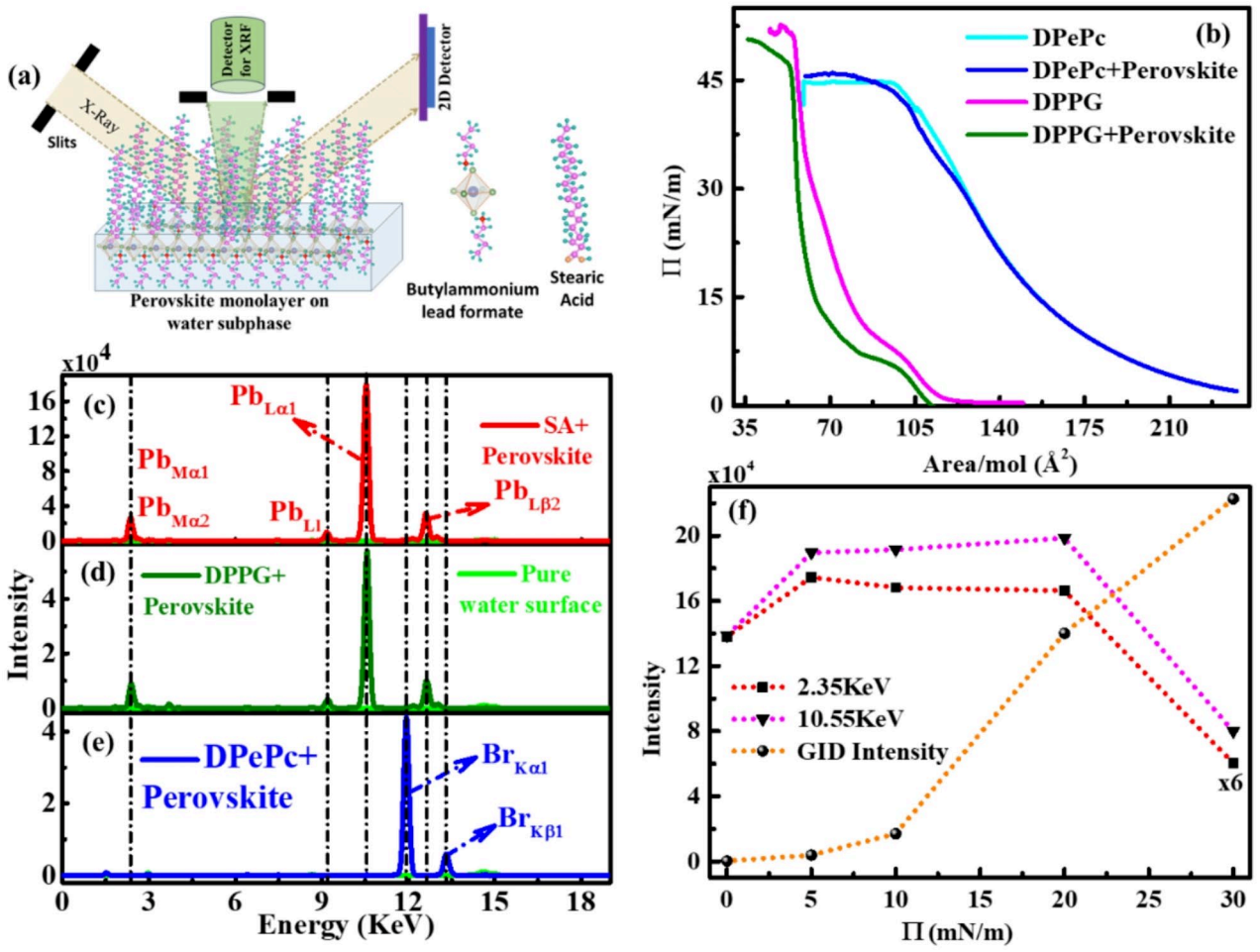

Fig. 1. (**a**) Schematic diagram of the x-ray scattering and x-ray fluorescence (XRF) measurement setup used to study the perovskite monolayer formation at the air-water interface. The models of butylammonium formate perovskite and stearic acid are also shown. (**b**) Isotherms of pristine DPPG (magenta), DPePC (cyan), DPPG + Perovskite (Olive), and DPePC + Perovskite (blue). Subtracted XRF data from (**c**) SA + Perovskite (red), (**d**) DPPG + Perovskite (Olive), (**e**) DPePC + Perovskite (blue) monolayer at the air-water interface. XRF data of only the water surface without the surfactants (green) is also shown. (**f**) The intensities from the peak of the GID scans (orange) and XRF spectra (red and magenta) are plotted as a function of surface pressure to show the appearance of the peak from the perovskite monolayer as the surface pressure increases. XRF spectrum of 2.35KeV is multiplied by 6 to show the nature of the curve in the same scale. All the molecular diagrams have been done using VESTA and ChemDoodle 3D software.

DMF solution of $(BA)_2PbBr_4$ was added to the water subphase confirming that the presence of the perovskite molecules at the water surface is not significant.

Figure 1b shows the Π-A isotherms of 1,2-dipalmitoyl-sn-glycero-3-phosphoglycerol (DPPG), and 1,2-dipalmitoyl-sn-glycero-3-ethylphosphocholine (DPePC), lipids with and without the presence of $(BA)_2PbBr_4$ in the water subphase. The isotherm of SA molecules with and without perovskites is shown in Fig. S1. The phase transition from the liquid expanded phase to the condensed phase of the isotherm is much sharp for the DPPG molecules in presence of the perovskites compared to the pristine one but the changes with the DPePC lipids are barely visible indicating that the attachment of the perovskites with the head group of the lipids, if any, is insignificant to change the physical properties of the monolayer. But a drastic change in the Π-A isotherm (refer to Fig. S1) was observed as we spread the stearic acid (SA) solution in chloroform on the surface of water having $(BA)_2PbBr_4$ in the subphase. It is important to note that both the SA and DPPG molecules have negatively charged head groups while the lipid DPePC has a positively charged head group. So, the effect of charge and the head group elements play an important role in making molecular assembly with the perovskites. Molecular area of condensed state of SA molecules reduced from 22 $Å^2$ to 15 $Å^2$ in absence or presence of perovskite molecules respectively but no such significant changes have been observed in the case of both the lipids. Simultaneous measurement of XRF from the monolayer provide us with information regarding the presence of elemental species at the air-water interface. The appearance of Pb $M_{\alpha1}$, $M_{\alpha2}$, $L_{\alpha1}$, $L_{\beta2}$, $L_{\gamma1}$ as marked in Fig. 1c clearly indicates the presence of lead ions at the air-water interface. We observed (refer to Fig. 1f) strong intensity of Pb XRF peaks even at zero pressure (Π) confirming the self-initiated nature of the interfacial reaction that brings Pb ions from bulk water to the negatively charged SA or DPPG head groups at the water surface. The intensity of the GID peak due to the in-plane ordering of Pb ions that we shall discuss below is also plotted in Fig. 1f and we noticed that the GID intensity increases with pressure (Π) as the molecular area (A) is reduced. At higher pressure Pb ions occupy only designated sites in 2D perovskite structure at the water surface and excess Pb ions submerge in bulk water to reduce measured XRF intensity (refer to Fig. 1f).

Langmuir monolayers of the lipids DPPG and DPePC were compared with the SA monolayer to understand the role of the charge of the headgroups and the specificity of the SA headgroup in the formation of perovskites at the water surface. The DPPG monolayer having negatively charged head groups like SA molecules shows the Pb XRF peaks, but the intensity is much lower (refer to Fig. 1d) than that obtained from the SA monolayer. The Pb peaks in the case of DPPG + perovskite monolayer shows that the intensity is almost 2.5 times lower than that obtained from the SA + perovskite monolayer. In the case of DPPG, one PG headgroup is associated with two hydrocarbon chains occupying almost 2.5 times the average area available for the SA head group in the Langmuir monolayer configuration. The area mismatch of the DPPG head groups in comparison to the smaller head groups in SA results in a significantly lower negative charge density for the head groups of DPPG molecules than that of the SA molecules head groups which explains the observation of lower intensity for the Pb XRF in the case of DPPG monolayer. However, the situation is completely opposite for the DPePC molecules having positively charged head groups. We get the $K_{\alpha1}$, and $K_{\beta1}$ XRF-peaks for the Br ions at the air-water interface, and the peaks corresponding to Pb ions is not observed (refer to Fig. 1e). These observations show the effect of charge, and the head group structure can determine the complex structure formation of the molecules at the air-water interface.

In-situ measurements of XRR and GID from the air-water interface were carried out systematically to decipher the nature of the formed Langmuir monolayers with DPPG, DPePC and SA. These measurements give information regarding the thickness, the electron density profile (EDP) as a function of depth, the interfacial roughness, and the 2D in-plane structure of a film[11,40]. Here we used these techniques to understand the formation of the 2D structure of perovskites on the water surface and the subsequent changes in the monolayer due to the change in the headgroups of the surfactants. Representative XRR data from all the monolayers and corresponding EDPs are shown in Fig. 2a and the perovskites layer form at the head region of the surfactants are marked as H in the inset of Fig. 2a. In the extracted EDPs water surface is at Z = 0 Å and the floating tail (FT) region above the water surface for all monolayers is on the positive side of Z showing an average electron density of 0.34 electron/$Å^3$—a typical value of hydrophobic tail region on the water surface. SA monolayer without and with $(BA)_2PbBr_4$ in water are found to be very different—an increase in separation between two successive minima clearly shows the thickening of monolayer and a drastic change in the electron density of head-group (H) region confirms the formation of lead-containing perovskite monolayer at the water surface. The electron density of the H region in the SA monolayer without and with perovskites in the water subphase changes from (0.39 ± 0.05 electrons / $Å^3$) to (0.83 ± 0.05 electrons / $Å^3$) with almost no change in the thickness of this region. On the other hand, DPPG + perovskite monolayer shows an expanded H region in water just below the surface with a significant increase in the electron density of the H region. DPPG has a bigger head group, so the head region layer thickness (∼ 8 ± 0.2 Å) is a little more than the same obtained for the SA + perovskite monolayer. Out of this 8 Å head group thickness, the upper part (just below the water surface) has an electron density of 0.43 ± 0.05 electron/$Å^3$ and the lower part has an electron density of 0.7 ± 0.05 electron/$Å^3$ as shown in the inset of EDP of Fig. 2a. This is due to the attachment of Pb ions with the terminal OH group of the head part of the lipid. The lower electron density of this region compared to the SA + perovskite monolayer implies a smaller number density of Pb ions attachment with the relatively large area available for the head groups of the DPPG lipids. This observation is consistent with the XRF intensity observed for the SA and DPPG monolayer with perovskite in the subphase as mentioned before. The length of the tail part of the DPPG molecule above the water surface is also found to have lower thickness compared to the SA molecules as DPPG has a lower number of carbon chains and higher tilt over the water surface compared to SA molecules. The extracted EDP from the DPePC + Perovskites monolayer shows a much lesser electron density in the head region compared to the values obtained in SA and DPPG monolayer with perovskites. This practically rules out the attachment of Pb ions with the head region of the DPePC lipids as observed in the XRF measurements from the DPePC monolayer. The tail

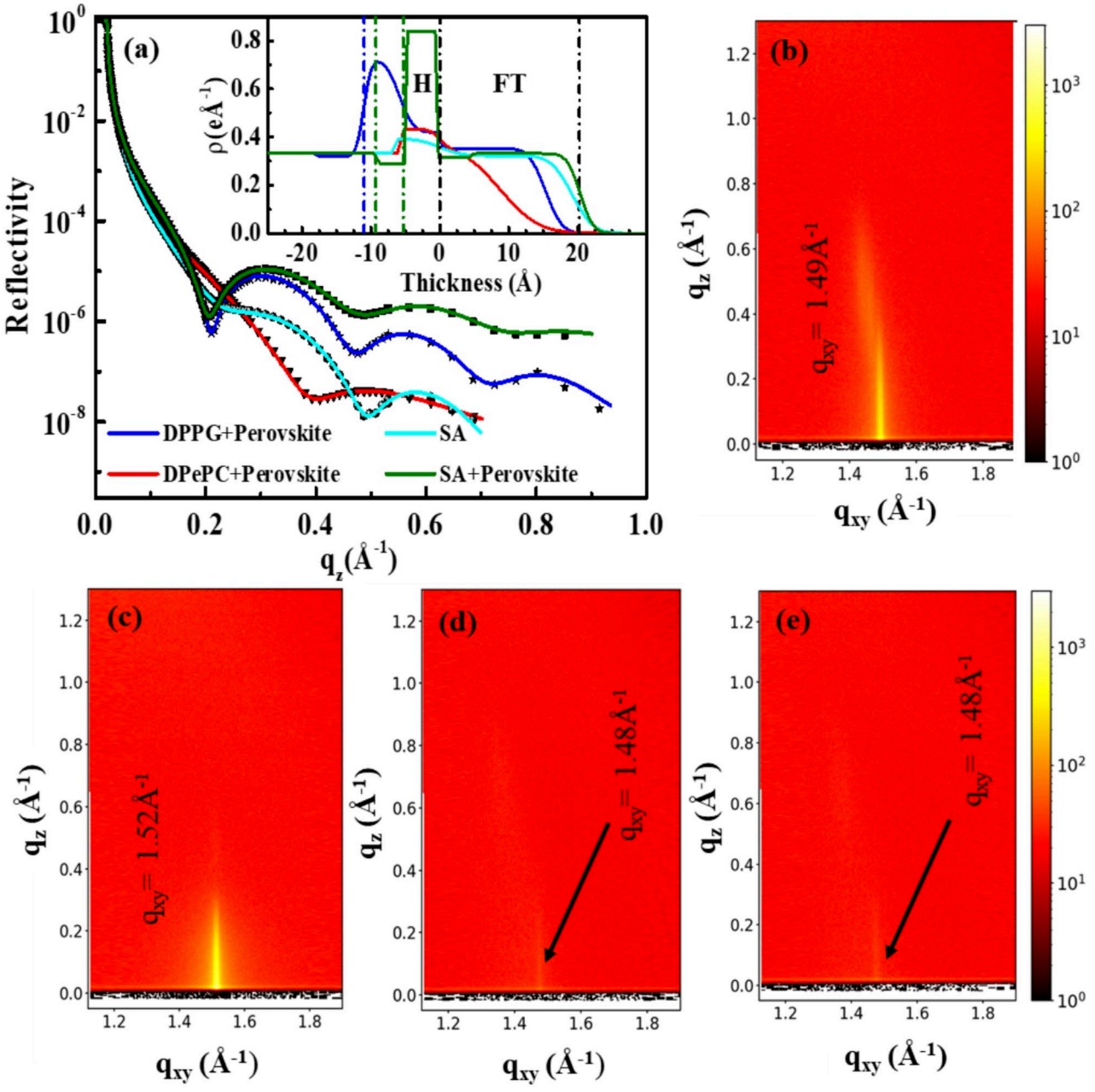

Fig. 2. (**a**) XRR profiles (symbols are experimental data and lines are the fitted profiles) of SA (Olive), DPPG (blue), and DPePC (red) monolayer on the water surface with perovskite in the water subphase at a surface pressure of 10 mN/m. XRR of pristine SA monolayer (cyan) at the same surface pressure and extracted EDP (cyan) is presented in (**a**). The inset shows corresponding electron density profiles (EDPs) obtained from fitting XRR data. H and FT indicate the head region and floating tail region respectively (refer to text for details). GID scan image of pristine DPPG (**b**), DPePC (**d**), perovskite mixed DPPG (**c**), and perovskite mixed DPePC (**e**) monolayer obtained from the air-water interface.

region electron density also shows bigger roughness implying the poor quality of monolayer formation than the monolayers formed by the negatively charged head group surfactants.

The GID data of the pristine DPPG, DPePC, and perovskite mixed monolayer are shown in Fig. 2b–e. The pristine DPPG monolayer also shows a similar GID pattern as observed for the pristine SA monolayer but here the two peaks are a little more separated than the SA monolayer peaks indicating more distortion in the in-plane centered hexagonal lattice for the DPPG molecules at the air-water interface. The GID image of the SA monolayer with perovskites in the subphase (refer to Fig. S3c,d) shows an additional peak corresponding to the lattice formation of Pb perovskites in the water. The GID peak at q_{xy} = 1.49 Å^{-1} for the pristine SA monolayer corresponds to the well-known[41] centered hexagonal in-plane lattice of the tails a_{st} = 4.77 ± 0.01 Å and the

additional in-plane peak appearing at q_{xy} = 1.71 Å^{-1} after perovskites attachment to SA molecules and this peak has almost constant intensity along the q_z direction indicating an infinite repeat distance in the real-space out-of-plane direction – the characteristics of the 2D lattice formation at the air-water interface as observed early[19].

We have plotted the intensity of the Pb lattice GID peak at q_{xy} = 1.71 Å^{-1} as a function of surface pressure in Fig. 1f in the same plot of XRF intensity to compare the growth of this peak as the monolayer surface pressure increases. The formation of the lattice of Pb ions starts at the onset of pressure build-up for the hybrid monolayer and once it forms a complete lattice around the pressure of 10 mN/m, the intensity increases linearly as per the contribution of populating domains within the footprint of the x-ray beam on the monolayer assembly. In the case of the pristine DPPG monolayer, the observed GID pattern (refer to Fig. 2b) is similar to the pristine SA monolayer (Fig. S3c). But in the presence of perovskites in the subphase, the DPPG monolayer shows only a single sharp peak at q_{xy} = 1.52 Å^{-1} corresponding to the centered hexagonal in-plane lattice of the tails of the lipid chains (refer to Fig. 2c). The Pb lattice peak is not observed for the monolayer of DPPG with perovskites in the subphase. In other case, a very weak peak is observed at q_{xy} = 1.48 Å^{-1} corresponding to pristine and perovskite mixed DPePC lipid monolayer (Fig. 2d,e) as it does not form any perovskite structure on water surface.

If we consider the number of electrons of one octahedral structure of perovskite molecule, $PbBr_4$, present in 19.7 Å^2 (as obtained from GID scan) and further assume that only two in-plane halogens (actually four that are shared in-plane) are counted in the H region thickness of 5.5 Å (as obtained from XRR profile), the electron density in the H region comes out to be 2.05 electrons / Å^3. This density is significantly higher than the density obtained from XRR of 0.83 electrons / Å^3 of this head region of the assembly. But if we just consider the formation of $Pb(HCOO)_4$ and count similarly two in-plane pseudohalides the electron density in the H region comes out to be 1.18 electrons / Å^3 which is quite close to the density obtained from the XRR analysis. This observation points to the fact that there is a possibility of the formation of lead formate by replacing the Br atoms from the perovskite structure with the $HCOO^-$ coming from the SA monolayer headgroups and to investigate this we have performed Raman spectroscopy from the LS films deposited on Si substrate.

Two-dimensional lead formate perovskite film

The transferred LS film forms a multilayer structure that exhibits Bragg peaks with a periodicity ~ 50 Å (refer to Fig. S3b). This multilayer assembly has been deposited from the vertical stacking ~ 25 Å monolayer structure at the air-water interface observed in the XRR data (refer to Fig. 2a).

The TEM image of the transferred film on a copper grid is shown in Fig. S4a and the corresponding EDX spectrum from a crystalline domain is shown in Figure S4(b).The EDX spectrum from one such crystalline domain shows the peaks corresponding to Pb ions apart from the Cu peaks coming from the grid material. It is important to note that no peaks corresponding to Br ions have been observed in this study and it is commensurate with the observation found from the XRF, and Raman scattering data to be discussed next. The LS films of DPPG + perovskites and DPePC + perovskites transferred on the TEM grid do not show any crystalline ordered domains as observed in the films prepared from SA + perovskites monolayer. The AFM images from the DPePC + perovskite and DPPG + perovskite LS films shown in Fig. 3(a) and (b) also do not show such formation of large domains in the film. To elucidate the dimensions more precisely, we extracted the line profiles from the AFM images around those domains as shown in Fig. 3c,d for the films from DPePC, and DPPG lipids with perovskites in the subphase respectively.

The vibrational modes of a HOIP obtained in Raman spectroscopy measurements are crucial for identifying the organic and inorganic species in perovskites[42,43]. The room temperature Raman spectra from the perovskite flakes (blue curve), perovskite LS thin film (red curve), and the bare Si substrate (cyan curve) used in both samples are shown in Fig. 4a–d. The relevant peaks corresponding to the Pb-Br band, or the formate group have been marked in the figures. Prominent Pb-Br in-plane and out-of-plane bond stretching found at 88 cm^{-1} and 104 cm^{-1} respectively for the $(BA)_2PbBr_4$ flakes are completely absent in the perovskite LS film (red curve) shown in Fig. 4a. The M5 band (122 cm^{-1} to 138 cm^{-1}) band coming from Pb-Br bond stretching observed for perovskite flake is also missing in the deposited LS film[42]. The fundamental internal vibrations of the formate perovskites and various modes of the symmetric and antisymmetric stretching of C–O, O–C–O bending, or C–H bending at different frequencies for different metal groups have been discussed earlier[43]. In our case, the bands ν_3, and ν_6 vibration modes for the $HCOO^-$ bonded with Pb are coming at 803 and 1064 cm^{-1} which matches well with the previously observed results for other metals. The bands ν_1 for the $HCOO^-$ have been found at 2848 and 2882 cm^{-1} which agrees well with the bands observed for Fe and Mg metals associated with $HCOO^-$. Though we are getting the Raman peaks corresponding to the $HCOO^-$ groups we have not received the signature peaks of the ketone group at around 1679 cm^{-1} and this observation rules out the formation of lead stearate at the air-water interface. It is also evident from the cyan and red spectra of Fig. 4a,b that the peaks found at 1000 cm^{-1} and between 50 cm^{-1} and 500 cm^{-1} originate from the Si substrate rather than the perovskite LS sample. The peaks at 814 cm^{-1}, 1295 cm^{-1}, and 1489 cm^{-1} in Fig. 4c,d corresponding to various modes of the NH_3 group of the BA are present in both the LS films and the $(BA)_2PbBr_4$ flakes. The absence of Pb-Br vibration mode peaks and the appearance of the vibration modes of $HCOO^-$ in the Raman spectra give clear proof of $(BA)_2Pb(HCOO)_4$ LS film formation at the water surface. We could not clearly resolve the shift in Pb-$HCOO^-$ vibration peaks in the Raman spectra due to strong Si background and small amount of nanometer thick lead-formate perovskites layer over the Si substrate (refer fitted data shown in the Fig. S5 and in the Fig. 4a). However, from this fitting we could detect Raman peaks at the 83 and 149 cm^{-1} for the Pb-formate perovskite films in our sample – these peak-positions are similar to those observed in the metal formate perovskites[43].

Photoluminescence (PL) measurements performed at temperatures 280 K and 4 K from the powder of perovskite flakes and deposited films of SA, DPPG, and DPePC are shown in Fig. 4e–h. The temperature-dependent PL measurements from the 2D flakes of $(C_4H_9NH_3)_2PbBr_4$ have been reported early[19]. Several studies have been performed to understand the rapid increase in band edge PL emission intensity with lowering

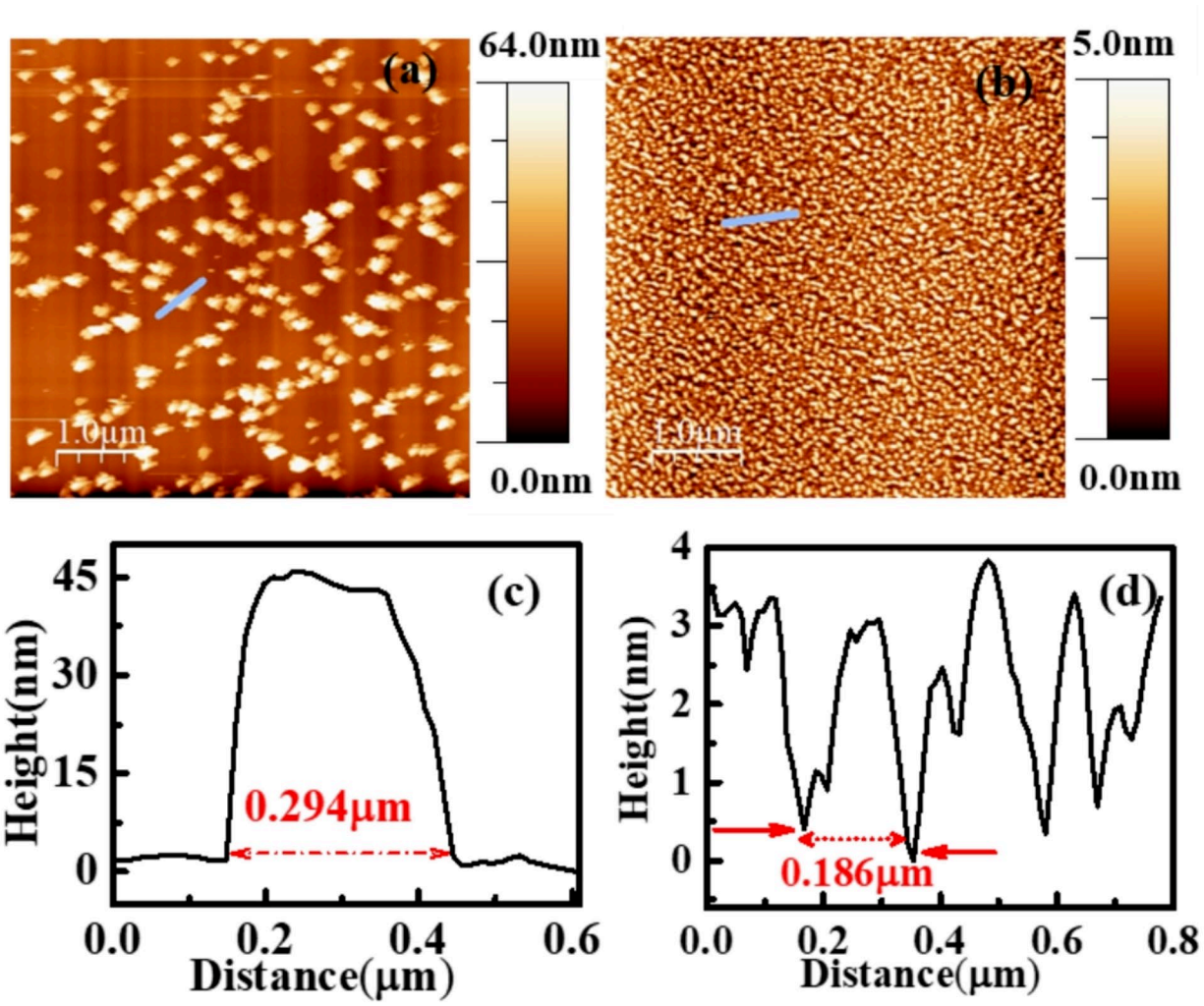

Fig. 3. (**a**) DPePC + perovskite, and (**b**) DPPG + perovskite film deposited on Si substrate. The height profile extracted from the respective AFM images is shown in (**c**), and (**d**).

temperature in HOIP materials based on underlying electron–phonon interaction[44]. We also observe (refer to Fig. 4e) two orders of magnitude increase in the PL peak at 414 nm for the powder of $(BA)_2PbBr_4$ flakes used in this study as the temperature reduced from 280 K to 4 K. In Fig. 4f, we have shown corresponding PL data for the $(BA)_2Pb(HCOO)_4$ LS film exhibiting a band-edge emission at 385 nm and a broadband emission spectrum with a peak at 450 nm as the temperature is lowered to 4 K. We observe around 5 times increase in intensity as the temperature is lowered from 280 K clearly indicating the intrinsic nature of broadband emission. The HOIP materials have exhibited such broadband emission due to static structural distortions related to out-of-plane tilting of the BX_6 octahedra[45]. It is to be noted that observed PL data is quite different from earlier reported $Pb(HCOO)_2$ films[46]. The LS film deposited from the DPPG monolayer also shows a very broad white band PL spectra but the intensity of the peak increases by only two times (refer to Fig. 4g) on lowering the temperature from 280 K to 4 K. The film prepared with DPePC lipids is not expected to form an HOIP structure and does not show much change in PL intensity with temperature indicating the optically inactive feature of the deposited films (refer Fig. 4h).

Conclusion

We have shown here that the Langmuir monolayer of lead formate perovskite can be formed at the air-water interface from the DMF solution of $(BA)_2PbBr_4$ and stearic acid monolayer. In-situ X-ray reflectivity, grazing incidence diffraction, and fluorescence measurements show the absence of bromine in the Langmuir monolayer and the presence of a single layer of lead. The $COOH^-$ that replaces Br^- in the 2D lattice of Pb comes from the stearic acid monolayer and is consistent with the earlier observation of SA dissociation that forms Heptadecane (HDCA) and formate[47]. The perovskite monolayer could be transferred on solid substrates as a multilayer structure, which exhibits excellent long-range order and shows expected Raman modes of formate perovskites. Other two lipid surfactants DPPG and DPePC do not show such perovskite layer formation at the air-water

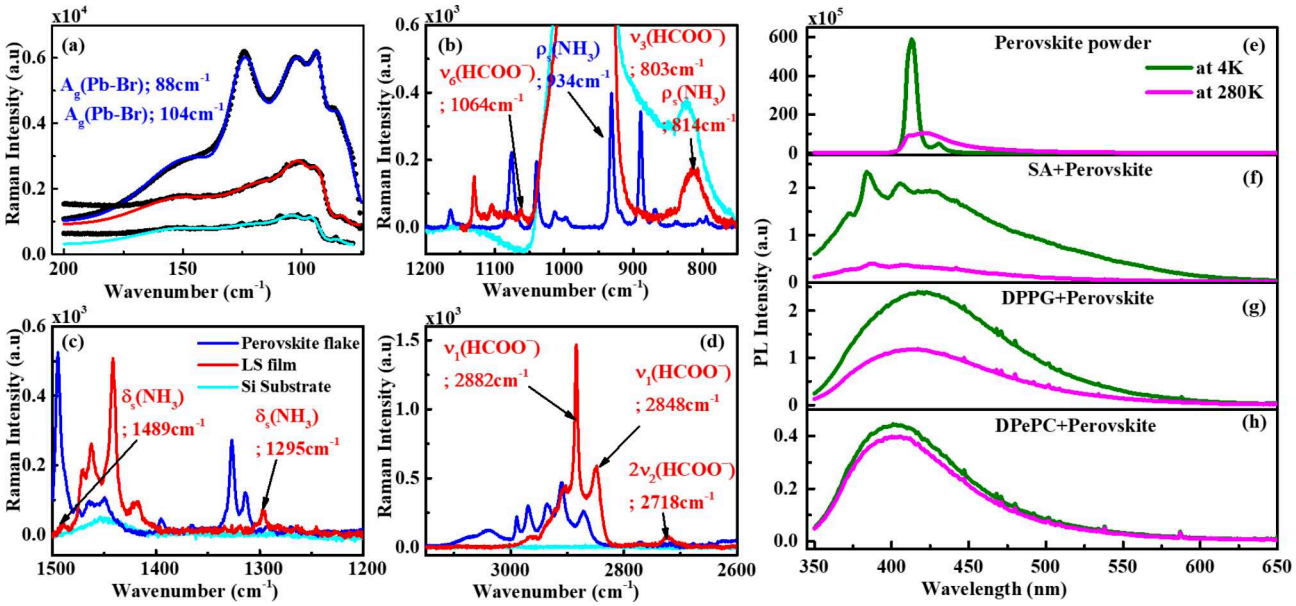

Fig. 4. The Raman spectra (**a**–**d**) measured at 300 K. Blue-coloured spectrum is from perovskite flakes, the red-coloured spectrum is from the perovskite mixed SA LS film, and the cyan-coloured spectrum is from the bare Si substrate. Experimental data points are in symbol and fitted data points are in line in (**a**). In all other (**b**–**d**), the lines are the experimental data points. PL spectra of the perovskite powder (**e**), the LS films deposited on Si (100) substrate from the monolayer of SA (**f**), DPPG (**g**), and DPePC (**h**) with perovskite in the subphase. The olive-coloured spectra are the PL spectra at 4 K and the magenta-coloured spectra are at temperature 280 K in all the figures for PL measurements.

interface in this mechanism. The measured PL data of this formate perovskite multilayer films exhibit broad-band white light emission across the entire visible range. The emission of white light from a single material is of interest for the development of solid-state lighting applications[45]. We plan to extend this investigation further to learn more about the details of the reaction at the air-water interface that forms formate perovskite monolayer with magnetic and nonmagnetic metal ions.

Data availability

Correspondence and requests for materials should be addressed to corresponding authors. The datasets used and/or analysed during the current study are available from the corresponding author upon reasonable request.

Received: 16 July 2024; Accepted: 29 October 2024
Published online: 20 February 2025

References

1. Tian, Y. M., Silva, W., Gschwind, R. M. & König, B. Accelerated photochemical reactions at oil-water interface exploiting melting point. *Depress. Sci.* **383**, 750–756 (2024).
2. Luo, G. et al. Ion distributions near a liquid-liquid interface. *Science* **311**, 216–218 (2006).
3. Sanyal, M. K., Sinha, S. K., Huang, K. G. & Ocko, B. M. X-ray-scattering study of capillary-wave fluctuations at a liquid surface. *PRL*. **66**, 628 (1991).
4. Benjamin, I. Chemical reactions and solvation at liquid interfaces: A microscopic perspective. *Chem. Rev.* **96**, 1449–1476 (1996).
5. Rao, C. N. R. & Kalyanikutty, K. The liquid–liquid interface as a medium to generate nanocrystalline films of inorganic materials. *Acc. Chem. Res.* **41**, 489–499 (2008).
6. Wang, Z. et al. On-water surface synthesis of charged two-dimensional polymer single crystals via the irreversible Katritzky reaction. *Nat. Synth.* **1**, 69–76 (2022).
7. Guo, Q., Xu, M., Yuan, Y., Gu, R. & Yao, J. Self-assembled large-scale monolayer of au nanoparticles at the air/water interface used as a SERS substrate. *Langmuir* **32**, 4530–4537 (2016).
8. Era, M. & Takada, N. Squeezed-out technique to prepare high-quality PbBr-based layered perovskite Langmuir–Blodgett films applicable to cavity polariton devices. *Langmuir*. **35**, 12224–12228 (2019).
9. Sanyal, M. K. et al. Formation and ordering of gold nanoparticles at the toluene – water interface. *J. Phys. Chem. C* **112**, 1739–1743 (2008).
10. Maiti, S. et al. Evidence of contact epitaxy in the self-assembly of HgSe nanocrystals formed at a liquid-liquid interface. *J. Condens. Matter Phys.* **29**, 095101 (2017).
11. Basu, J. K. & Sanyal, M. K. Ordering and growth of Langmuir–Blodgett films: X-ray scattering studies. *Phys. Rep.* **363**, 1–84 (2002).
12. Nielsen, J. A. et al. Principles and applications of grazing incidence X-ray and neutron scattering from ordered molecular monolayers at the air-water interface. *Phys. Rep.* **246**, 251–313 (1994).
13. Dou, L. et al. Atomically thin two-dimensional organic-inorganic hybrid perovskites. *Science*. **349**, 1518–1521 (2015).
14. Walker, B., Ma, B., Kim, G. H. & Kim, J. Y. Pseudohalides in lead-based perovskite semiconductors. *Adv. Mater.* **31**, 1807029 (2019).

15. Sasaki, T., Watanabe, M., Hashizume, H., Yamada, H. & Nakazawa, H. Macromolecule like aspects for a colloidal suspension of an exfoliated titanate. Pairwise association of nanosheets and dynamic reassembling process initiated from it. *J. Am. Chem. Soc.* **118**, 8329–8335 (1996).
16. Stranks, S. D. & Snaith, H. J. Metal-halide perovskites for photovoltaic and light-emitting devices. *Nat. Nanotechnol.* **10**, 391–4023 (2015).
17. Veldhuis, S. A. et al. Perovskite materials for light-emitting diodes and lasers. *Adv. Mater.* **28**, 6804–6834 (2016).
18. Leng, K., Fu, W., Liu, Y., Chhowalla, M. & Loh, K. P. From bulk to molecularly thin hybrid perovskites. *Nat. Rev. Mater.* **5**, 482–500 (2020).
19. Chowdhury, S. et al. Solution pro-cessed hybrid lead Perovskite films for white light emission and lasing applications. *Adv. Funct. Mater.* 2401334 (2024).
20. Saparov, B. & Mitzi, D. B. Organic–inorganic perovskites: Structural versatility for functional materials design. *Chem. Rev.* **116**, 4558–4596 (2016).
21. Boström, H. L. Tilts and shifts in molecular perovskites. *Cryst. Eng. Comm.* **22**, 961–968 (2020).
22. Ludi, A., Guedel, H. U. & Ruegg, M. Structural chemistry of prussian blue analogs. Single-crystal study of manganese (II) hexacyanocobaltate (III), $Mn_3[Co(DcN)_6]_2$. xH_2O. *Inorg. Chem.* **9**, 2224–2227 (1970).
23. Wu, Y. et al. [Am]Mn $(H_2POO)_3$: A new family of hybrid perovskites based on the hypophosphite ligand. *J. Am. Chem. Soc.* **139**, 16999–17002 (2017).
24. Ma, Y. & Sun, Y. Multiferroic and thermal expansion properties of metal-organic frameworks. *J. Appl. Phys.* 127 (2020).
25. Jain, P. et al. Multiferroic behavior associated with an order – disorder hydrogen bonding transition in metal – organic frameworks (MOFs) with the perovskite ABX_3 architecture. *J. Am. Chem. Soc.* **131**, 13625–13627 (2009).
26. Popoola, A. et al. First-principles property assessment of hybrid formate perovskites. *J. Chem. Phys.* **159**, 074702 (2023).
27. Boström, H. L., Bruckmoser, J. & Goodwin, A. L. Ordered B-site vacancies in an ABX3 formate perovskite. *J. Am. Chem. Soc.* **141**, 17978–17982 (2019).
28. Mitzi, D. B. Templating and structural engineering in organic–inorganic perovskites. *J. Chem. Soc. Dalton Trans.* **1**, 1–12 (2001).
29. Aguirre, L. C. G. et al. *Inorg. Chem.* **54**, 2109–2116. (2015).
30. Mączka, M. et al. Temperature- and pressure-Induced phase transitions in the Niccolite-type formate framework of $[H_3N(CH_3)_4NH_3][Mn_2(HCOO)_6]$. *J. Mater. Chem. C.* **4**, 3185–3194 (2016).
31. Chen, S., Shang, R., Hu, K. L., Wang, Z. M. & Gao, S. $[NH_2NH_3][M(HCOO)_3]$ (M = Mn_2^+, Zn_2^+, Co_2^+ and Mg_2^+): Structural phase transitions, prominent dielectric anomalies and negative thermal expansion, and magnetic ordering. *Inorg. Chem.* **1**, 83–98 (2014).
32. Yu, Z. et al. Pressure effect on order-disorder ferroelectric transition in a hydrogen-bonded metal-organic framework. *J. Phys. Chem. Lett.* **11**, 9566–9571 (2020).
33. Guo, Z., Wu, X., Zhu, T., Zhu, X. & Huang, L. Electron–phonon scattering in atomically thin 2D perovskites. *ACS Nano* **10**, 9992–9998 (2016).
34. Miura, Y. F., Akagi, Y., Hishida, D. & Takeoka, Y. Two-dimensional layered organic–inorganic hybrid perovskite thin-film fabrication by Langmuir–Blodgett and Intercalation techniques. *ACS Omega* **7**, 47812–47820 (2022).
35. Sheikh, T. & Nag, A. Mn Doping in Centimeter-Sized layered 2D butylammonium lead bromide (BA_2PbBr_4) single crystals and their optical properties. *J. Phys. Chem. C* **123**, 9420–9427 (2019).
36. Stoumpos, C. C. et al. Ruddlesden–Popper hybrid lead iodide perovskite 2D homologous semiconductors. *Chem. Mater.* **28**, 2852–2867 (2016).
37. Murphy, B. M. et al. A novel X-ray diffractometer for studies of liquid–liquid interfaces. *J. Synchrotron Rad.* **21**, 45–56 (2014).
38. Seeck, O. H. et al. The high-resolution diffraction beamline P08 at PETRA III. *J. Synchrotron Rad.* **19**, 30–38 (2012).
39. Shen, C., Kirchhof, R. & Bertram, F. *J. Phys.* **2380**, 012047 (2022).
40. Kaganer, V. M., Möhwald, H. & Dutta, P. Structure and phase transitions in Langmuir monolayers. *Rev. Mod. Phys.* **71**, 779–819 (1999).
41. Dupres, V. et al. Two-dimensional mixtures of stearic acid and partially fluorinated amphiphilic molecule: A grazing incidence X-ray diffraction study. *Langmuir*. **16**, 10189–10192 (2000).
42. Dhanabalan, B. et al. Directional anisotropy of the vibrational modes in 2D-layered perovskites. *ACS Nano* **14**, 4689–4697 (2020).
43. Mączka, M., et al. Phase transitions and coexistence of magnetic and electric orders in the methylhydrazinium metal formate frameworks. *Chem. Mater.* **29**, 2264–2275 (2017).
44. Zhang, F. et al. Brightly luminescent and color-tunable colloidal $CH_3NH_3PbX_3$ (X = br, I, cl) quantum dots: potential alternatives for display technology. *ACS Nano* **9**, 4533–4542 (2015).
45. Koegel, A. A. et al. Correlating broadband photoluminescence with structural dynamics in layered hybrid halide perovskites. *J. Am. Chem. Soc.* **144**, 1313–1322 (2022).
46. Gu, J. et al. Morphology tuning and its role in optimization of Perovskite films fabricated from a novel nonhalide lead source. *Adv. Sci.* **7**, 2002296 (2020).
47. Berenblyum, A. S., Podoplelova, T. A., Shamsiev, R. S., Katsman, E. A. & Danyushevsky, V. Ya. On the mechanism of catalytic conversion of fatty acids into hydrocarbons in the presence of palladium catalysts on alumina. *Pet. Chem.* **51**, 336–341 (2011).

Acknowledgements

Parts of this research were carried out at PETRA-III and we would like to thank Mr. Rene Kirchhof for technical support in using the beamline P08. M.K.S. acknowledges the support of the Indian National Science Academy Senior Scientist Programme. The authors acknowledge Mr. Sabyasachi Karmakar and Mr. Souvik Jana for scattering and AFM experiments respectively.

Author contributions

S.C., M.K.M., and M.K.S. have conceived the idea and planned the experiments. S.C., M.K.M, carried out the experiment and data collection at the P08 beamline of PETRA-III synchrotron DESY, Germany. S.C., M.K.M., and M.K.S. have contributed to sample preparation, analysis, interpretation of results, and manuscript preparation. R.P.G., B.B., C.S., and B.M.M. have given support at the P08 beamline during the experiment. B.S. has done TEM experiment. S.B. has given support for the PL and Raman experiment facility.

Funding

We acknowledge financial support by the Department of Science & Technology (DST), Government of India, provided within the framework of the India@Desy collaboration. We acknowledge DESY (Hamburg, Germany), a member of the Helmholtz Association HGF, for the provision of experimental facilities. Authors also like to acknowledge BMBF/05K16FK1/05K19FK2/ 05K21FK3 research grants for financing the LISA instrument, support, and the Lambda detector.

Declarations

Competing interests
The authors declare no competing interests.

Additional information
Supplementary Information The online version contains supplementary material available at https://doi.org/10.1038/s41598-024-78259-9.

Correspondence and requests for materials should be addressed to M.K.M. or M.K.S.